Charge−shift bonding in group IVB halides: A valence bond study of MH3−Cl (M = C, Si, Ge, Sn, Pb) molecules

ARTICLE *in* JOURNAL OF THE AMERICAN CHEMICAL SOCIETY · JANUARY 1999

Impact Factor: 12.11 · DOI: 10.1021/ja982218f

3 AUTHORS:

A. Shurki
Hebrew University of Jerusalem
49 PUBLICATIONS **1,308** CITATIONS
SEE PROFILE

Philippe C Hiberty
Université Paris-Sud 11
110 PUBLICATIONS **3,938** CITATIONS
SEE PROFILE

Sason Shaik
Hebrew University of Jerusalem
527 PUBLICATIONS **20,677** CITATIONS
SEE PROFILE

Charge-Shift Bonding in Group IVB Halides: A Valence Bond Study of MH_3−Cl (M = C, Si, Ge, Sn, Pb) Molecules

Avital Shurki,[†] Philippe C. Hiberty,*[,‡] and Sason Shaik*[,†]

Contribution from The Department of Organic Chemistry and the Lise Meitner-Minerva Center for Computational Quantum Chemistry, Hebrew University, 91904 Jerusalem, Israel, and The Laboratoire de Chimie Théorique (associated with the CNRS UA 506), Bât 490, Université de Paris-Sud, 91405 Orsay Cedex, France

Received June 25, 1998. Revised Manuscript Received November 16, 1998

Abstract: Charge-shift bonds form a distinct class of bonds where all or most of the bond energy is provided by the resonance energy between the covalent and ionic structures of the bond. This phenomenon is not associated with bond polarity, and charge-shift bonds exist among homonuclear (e.g., F_2, O_2) as well as heteronuclear cases [Sini, G.; Maitre, P.; Hiberty, P. C.; Shaik, S. S. *J. Mol. Struct. (THEOCHEM)* **1991**, *229*, 163. Shaik, S.; Maitre, P.; Sini, G.; Hiberty, P. C. *J. Am. Chem. Soc.* **1992**, *114*, 7861. Lauvergnat, D.; Hiberty, P. C.; Danovich, D.; Shaik, S. *J. Phys. Chem.* **1996**, *100*, 5715. Shaik, S. S. In *Molecules in Natural Science and Medicine;* Maksic, Z. B., Eckert-Maksic, M., Eds.; Ellis-Horwood, New York, 1991]. Valence bond (VB) computations performed on MH_3−Cl (M = C, Si, Ge, Sn, Pb) show that M−Cl is a "charge-shift bond" for which the major contribution to bonding arises from the resonance energy between the covalent M· − ·Cl (**1**) and ionic M^+:Cl^- (**2**) structures. The computations show that the strongest bond is Si−Cl while C−Cl is the weakest or the second weakest in the series. A detailed analysis shows that the root cause for the emergence of charge-shift bonding and the associated chemical manifestations is the joint behavior of the covalent and ionic VB constituents. Thus, repulsive interactions raise the covalent structure in energy, while enhanced electrostatic stabilization along with some π-back-bonding lowers the energy of the ionic structure. The covalent bonding is so meager that the major source of bonding must arise from the covalent−ionic resonance energy, i.e., the charge-shift resonance. Thus, for example, the root cause of the strong Si−Cl bonding originates in the energy proximity of its constituent VB structures and the near coincidence of their energy minima, which lead to a very large charge-shift resonance energy. Due to the large resonance energy, charge-shift bonds may possess high ionic charge distribution, but their ionicity remains virtual with no practical expression. Manifestations of charge-shift bonding are discussed, i.e., the rarity of free R_3M^+ cations for M = Si, Ge, Sn, and Pb, and the tendency of Sn and Si to form hypercoordination. The generality of this paradigm is discussed.

I. Introduction

The electron-pair bond is among the fundamental concepts of chemistry,[1] and is associated with the classification of bonding in terms of two generic paradigms, "covalent" (which include nonpolar and polar-covalent bonds) and "ionic". This classification has dominated chemical epistemology now for a few decades, and has been substantiated on a firm experimental basis. Theoretically, these paradigms have been described by valence bond (VB) theory[2] by appeal to the corresponding VB configurations, depicted in Scheme 1. Thus, the covalent bond, be it *polar or nonpolar*, is regarded as the class where most of the bond energy arises from the spin-pairing of the shared electrons in the covalent Heitler−London[3] form, A· − ·B (**a**), where the electrons are localized on their fragments and are allowed to exchange their spins, thereby resulting in energy lowering and bonding.[4] In contrast, an ionic bond is considered

Scheme 1

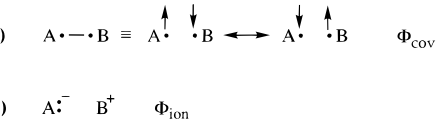

as the type where the bond energy originates mostly, if not only, from the electrostatic stabilization of the ionic VB form, A^+:B^- (**b**).

Despite the great utility of these paradigms, they do not describe essential bonding features, to begin with in homonuclear bonds such as F−F, O−O, and N−N.[5a,b] Thus, for example, in F_2, with zero charge separation, the covalent bond energy (due to the Heitler−London structure) is negative, and the molecule is bonded by the resonance energy between the covalent structure and the fluctuating ionic forms. Following this finding,[5a] it has become apparent that alongside the traditional covalent (polar-covalent) and ionic bond types, one must consider electron-pair bonds, both homo- and heteronuclear, which are neither covalent nor ionic in the above sense.

[†] Hebrew University.
[‡] Université de Paris-Sud.

(1) (a) Lewis, G. N. *J. Am. Chem. Soc.* **1916**, *38*, 762. (b) Langmuir, I. *J. Am. Chem. Soc.* **1919**, *41*, 868, 1543.

(2) Pauling, L. *The Nature of the Chemical Bond*, 3rd ed.; Cornell University Press: Ithaca, NY, 1960.

(3) Heitler, W.; London, H. F. *Physik* **1927**, *44*, 455.

(4) Shaik, S. S. In *New Theoretical Concepts for Understanding Organic Reactions*; Bertrán, J., Csizmadia, I. G., Eds.; Kluwer Academic Publishers: Dordrecht, The Netherland, 1989; Vol. C267.

10.1021/ja982218f CCC: $18.00
Published on Web 01/20/1999

The raison d'être of these bonds is the resonance interaction energy between the covalent and ionic forms, and this feature is associated with distinct properties, such as depleted electron density in the bonding region of F_2,[5b] extensive charge separation, e.g., in Si−X with no practical manifestations of ionic chemistry,[5c] etc. We have proposed to call this bond type *a "charge-shift bond" since its bonding derives, primarily if not only, from the fluctuation of charge inherent in the resonance between the two bonding forms (Scheme 1)*.

Following the initial studies we[5] and others[6] have encountered charge-shift bonding in a variety of molecules, e.g., X−F (X = F, H, CH_3, SiH_3),[5a,b] HO−OH,[5b] CH_3−OH,[6] H_2N−NH_2,[5b] CH_3−NH_2,[6] and SiH_3Cl,[5c] and in ion−molecular bonds as in the CH_3−NH_3^+ species.[5d] The same bonding type was observed also for hypercoordinated species and transition structures, e.g., $(FHF)^-$, $(FCH_3F)^-$, and $(FSiH_3F)^-$[5b,e] Thus, the existence of this bonding feature in homonuclear molecules, on one hand, and the lack of charge shift bonding in some polar bonds (such as LiH which possesses an equal mixture of ionic and covalent structures),[5a] on the other, demonstrate clearly that *charge-shift bonding is a class by itself not associated necessarily with bond polarity*[7] *in the traditional sense of Pauling or Sanderson*. Furthermore, the variety of species which have been found so far to exhibit charge-shift bonding indicate that this bonding type may constitute a significant, if not a prevalent, bonding form in chemistry. To explore further the range of applicability of this bonding paradigm and to outline its possible chemical manifestations, in the present paper we follow a preliminary study,[5c] and investigate by means of VB ab initio calculations[8] the M−Cl bond in the series of MH_3−Cl bonds where M is a group IVB element: C, Si, Ge, Sn, and Pb.

There are more reasons than one to study this series. First, it is concerned with bonding of first vs higher row atoms which is a fundamental problem[9] that has gained renewed attention in recent years.[10−12] Thus, it has been demonstrated by Schleyer et al.[12a] and by Apeloig[11] that C−X bonds are stronger than corresponding Si−X bonds, when X is not an electronegative group, such as H, CH_3, etc. In contrast, for electronegative X groups (such as X = F, OR, Cl, Br, I, etc.), the stronger bond becomes Si−X.[11,12a] It was concluded that these relative bond energies are influenced mainly by the electronegativity of the X group attached to C and Si. Subsequently Bickelhaupt et al.[12b] showed that the bond energy in the H_3M−Cl series (M = C, Si, Ge, and Sn) first increases from C to Si and then decreases. An energy component analysis revealed[12b] that this bond energy ordering is determined by an interplay of steric repulsion (due to Pauli repulsion) and orbital interaction terms, between the constituent fragments, and that the orbital interaction term is strongly affected by the electronegativity difference between M and Cl. As shall be demonstrated in our VB study, this bond energy ordering, as well as the electronegativity and Pauli repulsion effects, is associated with the charge-shift nature of the corresponding bonds, and rooted in the interaction resonance energy between the covalent and ionic structures of these bonds.

An intriguing observation is the ubiquity of ionic compounds of the type $R_3C^+X^-$ in the solid state,[13] as opposed to the rarity of analogous compounds for Si and Ge, and very likely also for Sn and Pb. Thus, for example, even a compound such as Ph_3SiClO_4 which appears initially as a superb candidate to be an ionic solid, $Ph_3Si^+ClO_4^-$, has a nice covalent Si−O bond[14] unlike the corresponding carbon compound which is an ionic solid, $Ph_3C^+ClO_4^-$.[15] This observation is all the more puzzling in view of the fact that charge distribution of Si−X, Sn−X, etc. show virtual ionicity, certainly more so than the corresponding C−X bonds.[16] This enigma is most likely associated also with the rare, and until recently elusive, free silicenium ion[11,17−20] SiR_3^+ which has been made only last year under strong steric protection of the Si center.[21] The same difficulty to observe free cations in the solution phase has been discussed recently for SnR_3^+ and GeR_3^+.[22] All this is of course in stark contrast with the highly developed carbocation chemistry in

(5) (a) Sini, G.; Maitre, P.; Hiberty, P. C.; Shaik, S. S. *J. Mol. Struct. (THEOCHEM)* **1991**, *229*, 163. (b) Shaik, S.; Maitre, P.; Sini, G.; Hiberty, P. C. *J. Am. Chem. Soc.* **1992**, *114*, 7861. (c) Lauvergnat, D.; Hiberty, P. C.; Danovich, D.; Shaik, S. *J. Phys. Chem.* **1996**, *100*, 5715. (d) Shaik, S. S. In *Molecules in Natural Science and Medicine*, Maksic, Z. B., Eckert-Maksic, M., Eds.; Ellis-Horwood: New York, 1991; Chapter 12. (e) Shaik, S.; Shurki, A. *Angew. Chem.*, in press.

(6) Basch, H.; Aped, P. Hoz, S. *Mol. Phys.* **1996**, *89*, 331.

(7) In response to a comment made by a reviewer, we focus the distinction between the charge-shift bonding concept and the traditional polar-covalency ideas of Pauling (ref 2) and Sanderson (ref 47). While so doing, we note that, in all fairness, this cannot be construed as a criticism since the charge-shift bonding idea has been noticed (ref 5a) due to the facility of VB ab initio computations, which were not available at the times of either Pauling or Sanderson. In Pauling's VB treatment (ref 2) the entire bond energy of homonuclear bonds is taken as a covalent bond energy and used to estimate the polar contribution of heteronuclear bonds. This is never true, and is especially striking in the case for, e.g., F−F and O−O, where the covalent structure is unbound, i.e., *has a negative covalent bond energy*. So the Pauling formula for an A−B bond energy, which uses a geometric mean of the homonuclear bond energies ($(D_{A-A}D_{B-B})^{1/2}$) as the covalent energy (D_{cov}) of the polar bond, ignores completely the charge-shift nature of the homonuclear bonds and would severely underestimate the effect in all polar bonds, under any formulation of D_{cov}. Sanderson's work of polar covalence (ref 47) does not consider charge-shift bonding. Sanderson's equation predicts bond energies as a blend of covalent and ionic contributions ($E_{bond} = t_{cov}E_{cov} + t_{ion}E_{ion}$), while ignoring completely the charge-shift resonance between the ionic and covalent forms.

(8) Verbeek, J.; Langenberg, J. H.; Byrman, C. P.; Van Lenthe, J. H. TURTLE−ab-initio VB/VBSCF/VBCI program, Theoretical Chemistry Group, Debye Institute, University of Utrecht, 1993.

(9) Kutzelnigg, W. *Angew. Chem.* **1984**, *96*, 262; *Angew. Chem., Int. Ed. Engl.* **1984**, *23*, 272.

(10) See for example recent extensive reviews: (a) Patai, S.; Rappoport, Z. *The Chemistry of organic Silicon Compounds*; Wiley and Sons: Chichester, England, 1989; Vols. 1 and 2. (b) Patai, S. *The Chemistry of organic Germanium, Tin and Lead Compounds*; Wiley and Sons: Chichester, England, 1995.

(11) Apeloig, Y. Theoretical Aspects of Organosilicon Compounds. Vol. 1, Chapter 2 in ref 10a.

(12) (a) Luke, B. T.; Pople, J. A.; Krogh-jespersen, M.-B.; Apeloig, Y.; Chandrasekhar, J.; Schleyer, P. v. R. *J. Am. Chem. Soc.* **1986**, *108*, 260. (b) See recent analysis of H_3M−Cl (M = C, Si, Ge, Sn) using DFT: Bickelhaupt, F. M.; Ziegler, T.; Schleyer, P. v. R. *Organometallics* **1996**, *15*, 1477.

(13) Laube, T. *Acc. Chem. Res.* **1995**, *28*, 399.

(14) Prakash, G. K. S.; Keyaniyan, S.; Aniszfeld, S. K. R.; Heiliger, L.; Olah, G. A.; Stevens, R. C.; Choi, H.-K.; Bau, R. *J. Am. Chem. Soc.* **1987**, *109*, 5123.

(15) Gomes de Mesquita, A. H.; MacGillavry, C. H.; Eriks, K. *Acta Crystallogr.* **1965**, *18*, 437.

(16) (a) Gronert, S.; Glaser, R.; Streitwieser, A., Jr. *J. Am. Chem. Soc.* **1989**, *111*, 3111. (b) Reed, A. E.; Weinstock, R. B.; Weinhold, F. *J. Chem. Phys.* **1985**, *83*, 735. (c) Wiberg, K. B.; Wendolowski, J. J. *J. Phys. Chem.* **1984**, *88*, 586.

(17) (a) Apeloig, Y.; Stanger, A. *J. Am. Chem. Soc.* **1987**, *109*, 272. (b) Apeloig, Y. *Stud. Org. Chem.* **1987**, *31*, 33.

(18) (a) Lambert, J. B.; Kania, L.; Zhang, S. *Chem. Rev.* **1995**, *95*, 1191 (b) Schleyer, P. v. R. *Science* **1997**, *275*, 39.

(19) (a) Schleyer, P. v. R.; Buzek, P.; Müller, T.; Apeloig, Y.; Siehl, H.-U. *Angew. Chem.* **1993**, *105*, 1558; *Angew. Chem., Int. Ed. Engl.* **1993**, *32*, 1471. (b) Steinberger, H.-U.; Müller, T.; Auner, N.; Maerker, C.; Schleyer, P. v. R. *Angew. Chem.* **1997**, *109*, 667; *Angew. Chem., Int. Ed. Engl.* **1997**, *36*, 626.

(20) Xie, Z.; Bau, R.; Benesi, A.; Reed, C. A. *Organometallics* **1995**, *14*, 3933.

(21) Lambert, J. B.; Zhao, Y. *Angew. Chem.* **1997**, *109*, 389; *Angew. Chem., Int. Ed. Engl.* **1997**, *36*, 400.

(22) (a) See, Cremer, D.; Olsson, L.; Reichel, F.; Kraka, E. *Isr. J. Chem.* **1993**, *33*, 369. (b) See however: Sekiguchi, A.; Tsukamoto, M.; Ichinohe, M. *Science* **1997**, *275*, 60. (c) Jemmis, E. D.; Srinivas, G. N.; Leszczynski, J.; Kapp, J.; Korkin, A. A.; Schleyer, P. v. R. *J. Am. Chem. Soc.* **1995**, *117*, 11361.

Scheme 2

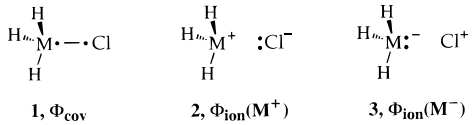

solution. A rationale based on the charge-shift bonding paradigm will be proposed to account for these intriguing trends.

Another question which can be posed for the target series of our study is the relative importance of π-back-bonding in molecules which are formally σ-bonded. This π-back-bonding via hyperconjugation[11,23] seems to be important for Si in the siloxane bond (Si−O−Si), which has a wide open angle up to 180°. Not much is known about this feature in the other elements of group IVB, except perhaps for the recent theoretical investigation of Basch and Hoz,[24,25] which indicates that Si seems to be more prone than the other group IVB elements to participate in hyperconjugative π-back-bonding. A related observation is the tendency which peaks for Si and Sn to form hypercoordination compounds,[26] an issue which is related to the debates regarding the role of valence-shell expansion via d orbital participation.[9,27,28] We will try to show how hypercoordination is sustained by charge-shift bonding.

Finally, as we move down a column of the periodic table, the atomic properties do not vary in a monotonic fashion. Thus, in C, the more extended valence orbital is 2s while 2p is somewhat smaller, due to the repulsion of 2s with the $1s^2$ core.[9] Moving on to Si, both 3s and 3p valence orbitals increase, the latter more than the former. Ge exhibits a break in the trend due to the imperfect screening of the $3d^{10}$ shell, which causes the so-called "transition metal contraction"[29] leading to contraction and energy lowering of the 4s orbitals and to a limited extent also of the 4p orbital. In Sn, the 5s and 5p orbitals increase and rise in energy again. This is followed by a drop in Pb, in which the 6s and less so the 6p orbitals contract due to the "lanthanide and relativistic contractions".[29] How would these atomic properties express themselves in the bond strength and specifically in the M−Cl bond strength (M = C → Pb), which is the target in this study?

In this paper we use VB computations and theoretical modeling to address the above issues, by looking at the MH_3−Cl bond in terms of the three constituent VB structures **1**−**3**, in Scheme 2. The first, Φ_{cov} **1**, describes the covalent Heitler-London[3] type configuration while the other two, **2** and **3**, are the ionic structures designated as $\Phi_{ion}(M^+)$ and $\Phi_{ion}(M^-)$ in accord with the charge on the MH_3 moiety. As shall be seen, these bonds as well as many of their properties, subscribe to the *charge-shift bonding* paradigm.

II. Methodology

The coupled cluster method, CCSD(T), which includes singles and doubles, and perturbation correction due to triples,[30] and which is known to provide reliable bond energies, is chosen as the benchmark method. Thus, the results of the three configuration VB calculations will be routinely monitored against CCSD(T) results within the same basis set. Should the results be the same for a given basis set, then the performance of the VB methods will be deemed reliable, and a bonding mechanism may be derived by reference to the compact VB wave function.

MO and VB Software. The coupled cluster calculations, e.g., CCSD(T), CCSD,[31] etc., were performed with the GAUSSIAN 94[32] series of programs. VB calculations were carried out using the Utrecht package TURTLE,[8] which is a general nonorthogonal CI program that performs simultaneously linear variation and orbital optimization on a given set of VB configurations. The orbital optimization is based on the super-CI technique[33a,b] related to the generalized Brillouin theorem.[33c]

Effective Core Potentials (ECPs) and Basis Sets. The study used valence only orbitals, where the core is replaced by either a relativistic or a nonrelativistic effective core potential (ECP). The relativistic ECP involves the scalar relativistic effects[29] and spin−orbit-averaged orbitals. On the basis of previous experience, a split-valence basis set which includes polarization functions is sufficient to produce reasonably good bond energies by the VB method. Apart from economical reasons to avoid very large basis sets that contain highly diffuse and/or high-angular-momentum functions, such basis functions are not recommended from a conceptual point of view since they do not really qualify as atom-centered and their use spoils the original sense of "a VB structure".[34]

As a standard atomic ECP/basis set combination, we used the Hay−Wadt ECP along with the corresponding LANL2DZ[35a] split-valence basis set, augmented by d-polarization functions taken from Pople's 6-31G(d). The results using this ECP/basis set combination will be designated as BSI. Some of the calculations were repeated using the Stuttgart ECP and basis set,[35b] again with addition of d-polarization functions taken from Pople's 6-31G(d). The corresponding results will be designated as BSII. The recent results of Basch[25] indicate that PbH_3−Cl requires a triple-ζ (TZ) basis set that includes diffuse and double polarization functions, TZ(2d,1p,++). Therefore, we added the auxiliary double polarization and diffuse functions for the heavy atoms to BSI and recalculated PbH_3−Cl with the new basis set, hereafter BSI(2d,+). Adding diffuse and polarization functions to hydrogen was tested by use of the DZ(2d,1p,++) basis set. No extended basis set calculations were attempted for C → Sn, for which CCSD(T)/BSI gave compatible results with CCSD(T)/TZ(2d,1p,++).

Geometries. Complete geometry optimization for the MH_3−Cl (M = C, Si, Ge, Sn, Pb) compounds was carried out at the coupled-cluster CCSD(T)/BSI level. The one-dimensional coordinate for the VB potential energy curves involved only the M−Cl bond distance. All other geometric parameters for the H_3MCl molecules were determined at the GVB(1/2) level[36] by preoptimization at different M−Cl distances.

VB Methods. The VB wave function of a two-electron bond can be expressed in two ways: One is the traditional VB approach,[2] in

(23) (a) Albright, T. A.; Hoffman, P.; Rossi, A. R. *Naturforsch.* **1980**, *35b*, 343. (b) Sheldrick, W. S. Chapter 3 in ref 10a.
(24) Basch, H.; Hoz, T. Chapter 1 in ref 10b.
(25) Basch, H. *Inorg. Chim. Acta* **1996**, *252*, 265.
(26) Mackay, K. M. Chapter 2 in ref 10b.
(27) Reed, A. E.; Schleyer, P. v. R. *J. Am. Chem. Soc.* **1990**, *112*, 1434.
(28) Coulson, C. A. *Nature* **1969**, *221*, 1106.
(29) (a) Pyykkö, P. *Chem. Rev.* **1988**, *88*, 563. (b) Pyykkö, P. *J. Chem. Res. (S)* **1979**, 380.
(30) Rendell, A. P.; Lee, T. J. *J. Chem. Phys.* **1994**, *101*, 400.
(31) For CCD and CCSD(T) implemented in Gaussian 94 see: (a) Pople, J. A.; Krishnan, R.; Schlegel, H. B.; Binkley, J. S. *Int. J. Quantum Chem.* **1978**, *XIV*, 545. (b) Pople, J. A.; Head-Gordon, M.; Raghavachari, K. *J. Chem. Phys.* **1987**, *87*, 5968.
(32) Gaussian 94, Revision D.4: Frisch, M. J.; Trucks, G. W.; Schlegel, H. B.; Gill, P. M. W.; Johnson, B. G.; Robb, M. A.; Cheeseman, J. R.; Keith, T.; Petersson, G. A.; Montgomery, J. A.; Raghavachari, K.; Al-Laham, M. A.; Zakrzewski, V. G.; Ortiz, J. V.; Foresman, J. B.; Cioslowski, J.; Stefanov, B. B.; Nanayakkara, A.; Challacombe, M.; Peng, C. Y.; Ayala, P. Y.; Chen, W.; Wong, M. W.; Andres, J. L.; Replogle, E. S.; Gomperts, R.; Martin, R. L.; Fox, D. J.; Binkley, J. S.; Defrees, D. J.; Baker, J.; Stewart, J. P.; Head-Gordon, M.; Gonzalez, C.; Pople, J. A., Gaussian, Inc., Pittsburgh, PA, 1995.
(33) (a) Grein, F.; Chang, T. C. *Chem. Phys. Lett.* **1971**, *12*, 44. (b) Banerjee, A.; Grein, F. *Int. J. Quantum Chem.* **1976**, *10*, 123. (c) Levy, B.; Berthier, G. *Int. J. Quantum Chem.* **1968**, *2*, 307.
(34) Taking matters to an extreme situation, a single one-center expansion can be formally exact in an infinite basis set, but the wave function would not be interpretable in VB terms.
(35) (a) For first-row elements it uses D95: Dunning, Jr., T. H.; Hay, P. J. In *Modern Theoretical Chemistry*; Schaefer; H. F., III, Ed.; Plenum: New York, 1976; p 1. For higher row elements (Na−Bi) it uses Los-Alamos ECP plus DZ: Hay, P. J.; Wadt, W. R. *J. Chem. Phys.* **1985**, *82*, 270, 284, 299. (b) For C, Si, Ge, Sn, and Cl, see: Bergner, A.; Dolg, M.; Kuechle, W.; Stoll, H.; Preuss, H. *Mol. Phys.* **1993**, *80*, 1431.
(36) Bobrowicz, F. W.; Goddard, W. A., III. In *Modern Theoretical Chemistry: Methods of Electronic Structure Theory*; Schaefer, H. F., III, Ed.; Plenum: New York, 1977; Vol. 3, p 79.

which the wave function is described as a linear combination of one covalent and two ionic structures (e.g., **1**−**3** in Scheme 2), and where the bond electrons occupy pure atomic or hybrid orbitals. The alternative VB approach is provided by the GVB[36] or spin-coupled VB (SCVB)[37] theories, in which the bond is described by a single VB structure, formally covalent, but with orbitals that are allowed to delocalize freely and that might be considered as distorted atomic orbitals. At basic levels, the SCVB/GVB wave functions implicitly contain structures **1**−**3** which are explicitly used in the traditional VB wave function, and therefore the alternative wave functions are nearly equivalent. At such a level of theory, the SCVB/GVB option has the advantage of compactness, while the traditional description enables one to consider explicitly the covalent and ionic dissociation curves, and provides quantitative measure of the ionic−covalent resonance energies. At a more complex level of theory, which is essential for charge-shift bonding situations such as in the F_2 molecule,[38] both VB alternatives require treatment of dynamic correlation. In this respect, the GVB/SCVB wave function requires subsequent extensive CI treatment, while the traditional VB wave function can account for dynamic correlation effects, associated with bonding, and still maintains the compact three-structure VB description (see below). Therefore, in keeping with our goal to probe charge-shift bonding in M−Cl bonds, we can make use of the conceptual clarity of the three-structure VB wave function, as described below.

The VB potential energy curves and bond energies for the H_3MCl (M = C, Si, Ge, Sn, Pb) molecules were determined at various levels, starting with VBSCF and ending with BOVB.[38−40] In each case, the adiabatic VB wave function is a linear combination of the three configuration VB basis structures **1**−**3** in Scheme 2, as expressed in eq 1, where the *c* values are variational coefficients. Thus, each

$$\Psi(\mathrm{M-Cl}) = c_1\Phi_{\mathrm{cov}} + c_2\Phi_{\mathrm{ion}}(\mathrm{M}^+) + c_3\Phi_{\mathrm{ion}}(\mathrm{M}^-) \qquad (1)$$

configuration possesses an active space consisting of the electron pair in the M−Cl bond which is treated with correlation in the VB sense using localized M and Cl orbitals, and an inactive space composed of a set of doubly occupied orbitals due to the M−H bonds and Cl lone pairs. During the VB calculations all the orbitals as well as the coefficients of the covalent and the ionic structures (c_1−c_3, in eq 1) are optimized simultaneously. However, at any VB level the *active orbitals* are always kept strictly localized on their respective single atom or fragment. An important reason for this is that the strict localization of the active orbitals keeps the tractability of the VB structures in terms of classical structural formulas, in Scheme 2. A second reason is to avoid redundancy in the optimized parameters, since letting the orbitals delocalize in a formally covalent VB structure, **1**, would be equivalent to implicitly adding ionic structures, **2** and **3**. Such redundancy may lead to imbalance in a calculated potential surface, and in particular to overestimated bonding energies.[38] Finally, keeping the active orbitals localized enables one to deal with clearly defined diabatic states (e.g., ionic or covalent structures) that do not collapse to ground states by virtue of uncontrolled orbital optimization. The various VB levels differ, however, in the way the orbitals are optimized as discussed below.

At the VBSCF level all the orbitals are kept localized on their respective fragments, and are optimized as a common orbital set for the three VB structures. The VBSCF orbitals are therefore localized and respond to a mean field of the three VB structures, i.e., to an average neutral situation. We note that when the inactive orbitals are allowed to be delocalized in the VBSCF treatment, the resulting D-VBSCF bond wave function would be nearly equivalent to the one obtained from GVB/SCVB treatments, all corresponding to mean-field constraints.

Scheme 3

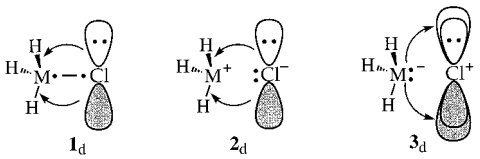

At the BOVB levels, this mean-field constraint is removed and each VB structure is allowed to have its own specific set of orbitals. As a result, the optimized orbitals are different from one structure to the other due to instantaneous response of the electrons to the local fields of the individual structures. The orbitals can be viewed as instantaneously following the charge fluctuation by rearranging in size and shape, hence the name "breathing-orbital valence bond" (BOVB).[39,40] Thus, the BOVB wave function accounts for some dynamic correlation during the bonding due to the charge fluctuation. The BOVB method has a few levels which differ in hierarchy of sophistication. Fuller details of the practical procedure to perform BOVB calculations at the various levels are given in the Appendix, while here we describe the key features of the methods.

The L-BOVB level is a BOVB analogue of the VBSCF wave function, where all orbitals are localized on their respective fragments, MH_3 or Cl, but are allowed to be different for the different VB configurations.

At the SL-BOVB level, the doubly occupied active orbitals in the ionic structures, **2** and **3**, are split,[5c,38,40] thereby allowing additional correlation of the two active electrons in the ionic structures. One might say that the SL-BOVB level provides the optimum bonding and dynamic correlation from a strictly localized orbital set.

Some delocalization or back-bonding is retrieved at the D-BOVB or the SD-BOVB levels, which allow the inactive orbitals to delocalize over the whole molecule. Scheme 3 depicts these effects in $\mathbf{1_d}$−$\mathbf{3_d}$, where it is seen that the delocalization dresses the structures with partial π-bonding due to hyperconjugative interactions between the p_π lone pairs of the Cl and the $\pi^*(MH_3)$ orbitals, or the $\pi(MH_3)$ orbitals and the diffuse vacant p_π(Cl). It is expected that the back-bonding will slightly change the charge character of the structure, but not in a drastic manner that will make the charge character unrecognizable. Of course, in a situation where π-bonding becomes of equal status to σ-bonding, the simple picture of the three VB structures should be replaced by a more complex picture which explicitly includes π-bonded VB structures. Such a situation, which may be recognized by the appearance of weights of individual structures much larger than unity or by completely altered charge character, has not been encountered in the present study.

Variationally Optimized VB Structures. When a single VB structure (**1**−**3** in Schemes 2 and 3) is allowed to optimize by itself, we obtain the variational energy of that structure. This energy is generally different from the energy of the same structure within the full 3 × 3 calculation, eq 1. Having variational energies of individual structures enables one to define variational values for conceptually important quantities such as covalent bond energy, charge-shift resonance energy, and individual π-bonding energies for the structures.

Weights of VB Structures and Charge Distribution. The weights of the VB structures are determined from the Coulson−Chirgwin[41] formula, eq 2, which is the VB analogue of the Mulliken population

$$w_i = c_i^2 + \sum_j c_i c_j S_{ij} \qquad (2)$$

analysis. Using Mulliken population analysis, it is also possible to obtain charge distributions for the individual VB structures, by specifying the basis functions which contribute to a certain group or atom (keyword

(37) (a) Cooper, D. L.; Gerratt, J.; Raimondi, M. *Adv. Chem. Phys.* **1987**, *69*, 319. (b) Cooper, D. L.; Gerratt, J.; Raimondi, M. *Int. Rev. Phys. Chem.* **1988**, *7*, 59. (c) Gerratt, J.; Cooper, D. L.; Raimondi, M. In *Valence Bond Theory and Chemical Structure*; Klein, D. J., Trinajstic, N., Eds.; Elsevier: New York, 1990; p 287. (d) Cooper, D. L.; Gerratt, J.; Raimondi, M. In *Advances in the Theory of Benzenoid Hydrocarbons;* Gutman, I., Cyvin, S. J., Eds. *Top. Curr. Chem.* **1990**, *153*, 41.

(38) For a recent review of the method, see: (a) Hiberty, P. C. In *Modern Electronic Structure Theory and Applications in Organic Chemistry*; Davidson, E. R., Ed.; World Scientific: River Edge, NJ, 1997; pp 289−367. (b) Hiberty, P. C. *J. Mol. Struct. (THEOCHEM)*, **1998**, *451*, 237.

(39) The BOVB method was developed first in Hiberty, P. C.; Flament, J. P.; Noizet, E. *Chem. Phys. Lett.* **1992**, *189*, 259.

(40) Further development and applications of BOVB using the package TURTLE[8] are discussed in (a) Hiberty, P. C.; Humbel, S.; Byrman, C. P.; Van Lenthe, J. H. *J. Chem. Phys.* **1994**, *101*, 5969. (b) Hiberty, P. C.; Humbel, S.; Archirel, P. *J. Phys. Chem.* **1994**, *98*, 11697.

(41) Chirgwin, H. B.; Coulson, C. A. *Proc. R. Soc. London, Ser. A* **1950**, *2*, 196.

Table 1. Equilibrium Bond Lengths $R(H_3M-Cl)$ (M = C, Si, Ge, Sn, Pb) (Å) at Various Levels for the Adiabatic, Covalent, and Ionic Curves

entry	method	M = C	M = Si	M = Ge	M = Sn	M = Pb
			Adiabatic, $R(3 \times 3)$			
1	exptl	1.781[a]	2.049[a]	2.149[a]	2.328[a]	
2	CCSD(T)[b]	1.780	2.044	2.166	2.344	2.413
3	SD-BOVB[c]	1.814	2.074	2.198	2.375	2.443
4	L-BOVB[c]	1.854	2.133	2.248	2.405	2.462
5	VBSCF[c]	1.866	2.138	2.244	2.401	2.460
			Covalent, R(cov)			
6	SD-BOVB[c]	1.810	1.966	2.120	2.325	2.418
7	L-BOVB[c]	1.924	2.068	2.200	2.398	2.492
8	D-BOVB[d]	1.834	1.981	2.126	2.333	
9	L-BOVB[d]	1.966	2.076	2.122	2.434	
			Ionic,[e] R(ion)			
10	SD-BOVB[c]	2.268	2.216	2.342	2.424	2.498
11	L-BOVB[c]	2.368	2.324	2.407	2.477	2.547
12	D-BOVB[d]	2.484	2.123	2.515	2.587	
13	L-BOVB[d]	2.552	2.387	2.695	2.712	

[a] From ref 53a−d, respectively, for M = C, Si, Ge, Sn, and Pb. [b] CCSD(T)/BSI//CCSD(T)/BSI. [c] The potential energy curve was calculated using BSI. The inactive geometric parameters are taken from GVB(1/2)/BSI. [d] The potential energy curve was calculated using BSII. The inactive geometric parameters are taken from GVB(1/2)/BSI. [e] The ionic structure is $H_3M^+Cl^-$.

= Mulliken). As a means to compare Mulliken populations with more acceptable analyses, we also performed natural population analysis (NBO).[42]

III. Results

The results are summarized in Tables 1−4 and in Figure 1.

Equilibrium Geometries. Table 1 shows the experimental and calculated values of the M−Cl bond distances (M = C, Si, Ge, Sn, Pb). The bond length progressively increases from C to Pb as expected due to the increase in the size of the central atom.[24,25] It is seen that the CCSD(T) bond lengths are close to the experimental ones, while the SD-BOVB results overestimate the bond lengths by, at most, ca. 0.05 Å. The VBSCF results are almost identical to the L-BOVB ones, implying that the dynamic correlation effect conferred by the breathing orbitals has a rather small affect on the geometry as might be expected. Both levels (VBSCF and L-BOVB) overestimate the bond length by about 0.1 Å relative to experiment. The improved bond lengths obtained by the SD-BOVB level highlight the bond-shortening effect of the π-back-bonding inherent to this level. The most significant bond shortening is observed for Si−Cl. Also shown in the table are covalent and ionic minima of the variationally optimized VB structures, $\mathbf{1}/\mathbf{1_d}$ and $\mathbf{2}/\mathbf{2_d}$. The latter quantities will be addressed later during the discussion.

Bond Energies, Back-Bonding, and Dynamic Correlation Effects. Table 2 shows the bond energies calculated at various VB/BSI levels, alongside coupled-cluster-calculated bond energies, and experimental values when available (entry 1 in the table).

For comparison, we show in entry 8 some CCSD(T) values calculated by Basch[25] using the Stevens−Basch−Kraus (SBK) ECP with a large basis set, TZ(2d,1p,++), of a triple-ζ doubly polarized quality augmented with sp diffuse functions on heavy atoms and s functions on the hydrogens. The CCSD(T) results with the two different ECPs and basis sets are virtually identical with the exception of Pb−Cl for which the smaller basis BSI, in entry 7, leads to a value 10.5 kcal/mol lower than the larger basis set in entry 8. It is thus clear that Pb is an atom which requires larger basis sets than C−Sn. However, recalculating the Pb−Cl bond energy using larger basis sets, i.e., BOVB/BSI(2d,+) and BOVB/BSI(2d,1p++), did not change the values obtained with the smaller basis set. The reason is that large basis sets for heavy atoms usually serve to account for angular electron correlation. This effect can be included in BOVB but at the expense of adding some extra VB structures, a complication that was not deemed essential in the present study. In any event, the computational results as well as experimental trends in analogous molecules (entry 1b) show that Si−Cl is the strongest bond, while C−Cl is either the weakest or the second weakest bond. This trend is contrary to nonpolar bonds, which are generally the strongest for the first period atom.[11,12a]

Table 2. Bond Energies D_e (kcal/mol) for MH_3-Cl (M = C, Si, Ge, Sn, Pb) at Various Levels

entry	method	M = C	M = Si	M = Ge	M = Sn	M = Pb
1a	exptl	87.3,[a] 83.4[b]	110.7,[a] 113[c]			
1b	exptl[d]	82	104	81	94	
2	VBSCF[e]	61.5	79.7	71.9	69.8	63.0
3	L-BOVB[e]	69.8	86.0	76.4	74.3	67.5
4	SL-BOVB[e]	71.6	87.5	78.2	76.1	69.5
5a	SD-BOVB[e]	80.1	102.1	88.6	84.6	76.3
5b	SD-BOVB[f]	79.9	101.7			
6	CCD[g]	76.9	98.5	87.9	83.7	75.0
7	CCSD(T)[h]	78.8	99.4	88.8	84.5	75.7
8	CCSD(T)[i]	76.5	99.2	89.4	87.6	86.2
9	GVB	69.4	88.0	77.8	78.2	69.8
	[VBSCF][j]	[68.3]	[89.2]	[80.1]	[76.6]	[68.2]

[a] D_e obtained from experimental D_0 values quoted in ref 54a and corrected by a calculated ΔZPE (ref 54b). [b] Calculated with ΔH_f^{298} values from ref 55. [c] Taken from ref 56. [d] Bond energies of $(CH_3)_3M-Cl$ molecules from ref 57. [e] Geometric values refer to Table 1. All calculations use BSI. [f] Taken from ref 5c. [g] From CCD/BSI//CCD/BSI. [h] From CCSD(T)/BSI//CCSD(T)/BSI. [i] Data taken from ref 25 and refer to CCSD(T)/ECP-TZ(2d,1p,++)//MP2/ECP-TZ(2d,1p) results. [j] Data in brackets are D-VBSCF values (VBSCF with delocalized inactive orbitals).

Comparison of the SD-BOVB trends to the benchmark CCSD(T) values, and to the available experimental data (entry 1a), shows agreement. Actually it is apparent that the accuracy of the SD-BOVB method is comparable to that of CCSD(T) (entries 5 and 7 for M = C, Si, Ge, and Sn). In general all VB methods including the lowest level (VBSCF, entry 2) predict the same trend noted before by Bickelhaupt et al.;[12b] i.e, changing the central atom from C to Si, the M−Cl bond energy increases dramatically but then decreases moderately and monotonically down the periodic table (M = Ge, Sn, Pb). Furthermore, comparison of the ECP results for C−Cl and Si−Cl in entry 5a to the previous all-electron results[5c] in entry 5b is also favorable. These are pleasing features of the VB method, that with a very compact wave function it picks most of the bonding energy between the fragments. Finally, the GVB values for the dissociation energies are also included in Table 2 (entry 9) for comparative purposes. It is seen that the GVB level (in which all the inactive orbitals are delocalized) is better than the simple VBSCF level (entry 2) which uses localized inactive orbitals. Permitting inactive orbital delocalization in VBSCF (see values in brackets in entry 9) shows the approximate equivalence of D-VBSCF and GVB. It is apparent, though, that the mean-field constraint in GVB and D-VBSCF gives consistently less accurate results in comparison with the best BOVB level (entry 5a); a manifestation of the importance of dynamic correlation associated with the breathing orbital effect.

(42) (a) Weinhold, F.; Carpenter, J. E. In *The Structure of Small Molecules and Ions*; Naaman, R., Veger, Z., Eds.; Plenum: New York, 1988; p 227. (b) Reed, A. E.; Curtiss, L. A.; Weinhold, F. *Chem. Rev.* **1988**, *88*, 899.

Table 3. Bonding Increments (kcal/mol) Relative to VBSCF

entry	M−Cl	*D*(VBSCF)	ΔE_{dyn}[a]	ΔE_{split}[b]	$\Delta E_{back-bond}$[c]
1	C−Cl	61.5	8.3	1.8	8.5
2	Si−Cl	79.7	6.3	1.5	14.6
3	Ge−Cl	71.9	4.5	1.8	10.4
4	Sn−Cl	69.8	4.5	1.8	8.5
5	Pb−Cl	63.0	4.5	2.0	6.8

[a] $\Delta E_{dyn} = D$(L-BOVB) − D(VBSCF). [b] $\Delta E_{split} = D$(SL-BOVB) − D(L-BOVB). [c] $\Delta E_{back-bond} = D$(SD-BOVB) − D(SL-BOVB).

Table 3 summarizes the bonding increment due to dynamic correlation, active orbital splitting, and π-back-bonding using the VBSCF results as the basic level. The dynamic correlation effect, in the second column, is seen to decrease down the group, from 8.3 kcal/mol for C−Cl to a virtually constant value of 4.5 kcal/mol for Ge−Cl to Pb−Cl. These results indicate that the dynamic correlation effect becomes less important as the outer valence orbitals increase in size down the periodic table.[38] The orbital splitting effect, in the second column, is rather small and virtually constant, ∼2 kcal/mol in all cases. In contrast, the delocalization effect due to π-back-bonding is significant in all cases (about 9−14% of the total bond energy), and is at a maximum for SiH_3Cl. Finally, we note that the VBSCF results reproduce the trends of the SD-BOVB level, and give about 80% of the SD-BOVB bond energy. In fact, bond energies can be obtained from the relation in eq 3, using a constant percentage

$$D = (5/4)D_{VBSCF} \tag{3}$$

of the VBSCF energy to account for the increments of dynamic correlation and back-bonding. While the actual increments are not truly constant, their sum does not vary much, so that the resulting bond energies from eq 3 are reasonable.

VB Potential Energy Curves. The VB energy curves at the SD-BOVB level are depicted in Figure 1 for the MH_3Cl molecules along the M−Cl coordinate (M = C, Si, Ge, Sn, Pb). While Figure 1 presents only the SD-BOVB results, it is noted that the same picture is projected by the lower VB levels as well. Each figure displays the curves for the adiabatic 3 × 3 state and the two lower and variationally optimized VB structures (Φ_{cov}, $\mathbf{1_d}$ and $\Phi_{ion}(M^+)$, $\mathbf{2_d}$). The covalent curve is seen to be bonded relative to the separate radicals in all cases.

It is interesting to note that the covalent structure is the lowest for C → Ge, whereas for Sn and Pb it is the ionic structure that becomes the lowest. It must be remembered, however, that while the variationally optimized structures have individually optimized energies irrespective of the other structures and their mixing, in the 3 × 3 adiabatic state the structures adapt themselves to produce the optimal configuration mixing. Indeed, as discussed below, all the bonds in the 3 × 3 calculations are dominated by the covalent structure. Nevertheless, it is apparent that the covalent and ionic curves are very close in energy especially for the heavier elements from Si to Pb.

The ionic curves in Figure 1 exhibit very deep wells, 134.3, 164.1, 156.6, 160.1, and 149.0 kcal/mol, relative to the separate ions in their relaxed geometry, for the CH_3Cl, SiH_3Cl, GeH_3Cl, SnH_3Cl, and PbH_3Cl, respectively. Curiously, the well depth variation mirrors the variation of the total bond energy, and does not vary monotonically; the shallowest well is for the lightest and presumably the smallest element, carbon.

VB Structures: Their Weights and Coefficients. A complimentary view of the VB mixing can be gained from the weights of the covalent Φ_{cov}, $\mathbf{1/1_d}$ and two ionic structures $\Phi_{ion}(M^+)$, $\mathbf{2/2_d}$ and $\Phi_{ion}(M^-)$, $\mathbf{3/3_d}$, collected in Table 4. The most reliable trends in the structural weights should be obtained from VBSCF or L-BOVB, since the delocalization effect in SD-BOVB confers π-covalency on the ionic structure and π-ionicity on the covalent structure. However, comparison of the SD-BOVB weights with the corresponding L-BOVB values shows few differences, suggesting that the π-back-bonding does not change the essential nature of the VB structures.

The major trend in the table is the dominance of the covalent structure in all the bonds. The second major structure is the normal-ionic one, $\Phi_{ion}(M^+)$, $\mathbf{2/2_d}$, while the weight of the inverse-ionic structure $\Phi_{ion}(M^-)$, $\mathbf{3/3_d}$ is negligible. Furthermore, at the BOVB levels for Si−Cl the latter weight is even negative, which in the Coulson−Chirgwin formula (eq 2) is interpreted as being simply very small. More puzzling is the negative sign of the corresponding coefficient,[43] which will be analyzed in the Discussion, while in the meantime we restrict our attention to the major structures, the covalent and normal-ionic.

Datum-by-datum inspection of the weights in Table 4 reveals some secondary trends in the weight of $\Phi_{ion}(M^+)$, $\mathbf{2/2_d}$, best projected by the VBSCF wave function. First, the trends in the ionic contribution follow the configuration energy gap in Figure 1; the smaller the gap, the larger the ionicity. The trend is not uniform, though, and moving from Si to Ge and then to Sn and Pb, the ionic weights (VBSCF, L-BOVB) exhibit a slight decrease, followed by an increase. This break in the monotonic trend is in line with the transition metal contraction expected in Ge due to the incomplete screening by the filled $3d^{10}$ subshell.[29] This trend is in good agreement with the population analysis results of Basch and Hoz[24] as well as with expectations from electronegativity scales, which suggest that the drop of electronegativity down group IVB exhibits an upward spike in Ge.[24,44]

IV. Discussion

The VB results reproduce the trends exhibited by the experimental data and coupled-cluster calculations. These trends are nascent from the mixing patterns of the covalent and ionic structures, **1**−**3** (Schemes 2 and 3). Let us therefore turn to understand these mixing patterns, and use the resulting bonding mechanisms to account for the various trends discussed in the Introduction.

A. Charge-Shift Bonding Mechanism for Group IVB Halides. A useful way to consider bonding is eq 4, which

$$D = D_{VBS} + RE_{cs} \tag{4}$$

expresses the bond energy as a sum of two terms, where D_{VBS} is the bond energy of the variationally optimized lowest VB structure, while RE_{cs} is the charge-shift resonance energy term due to the covalent−ionic mixing. The lowest VB structure is generally covalent, with the exception of Sn−Cl and Pb−Cl, where it is generally ionic (structure $\mathbf{2/2_d}$). In this form, all the terms in eq 4 are variational quantities, and the charge-shift resonance energy, RE_{cs}, is uniquely defined as the difference between the total bond energy and the maximum bonding potency given by a single VB structure.

These data are collected in Table 5. In most cases, but not

(43) For findings of negative mixing coefficients in MO mixing, see: (a) Whangbo, M. H.; Hoffmann, R. *J. Chem. Phys.* **1978**, *68*, 5498. (b) Ammeter, J. H.; Bürgi, H.-B.; Thibeault, J. C.; Hoffmann, R. *J. Am. Chem. Soc.* **1978**, *100*, 3686.

(44) (a) Pauling's scale updated by Allred in 1961: Allred, A. L. *J. Inorg. Nucl. Chem.* **1961**, *17*, 215. (The first version of Pauling's scale: Pauling, L. *J. Am. Chem. Soc.* **1932**, *54*, 3570.) (b) For Mulliken definition ($X_m = (I + A)/2$): Mulliken, R. S. *J. Chem. Phys.* **1934**, *2*, 782. (c) Allen, L. C. *J. Am. Chem. Soc.* **1989**, *111*, 9003 (d) Allred, A. L.; Rochow, E. G. *J. Inorg. Nucl. Chem.* **1958**, *5*, 264, 269.

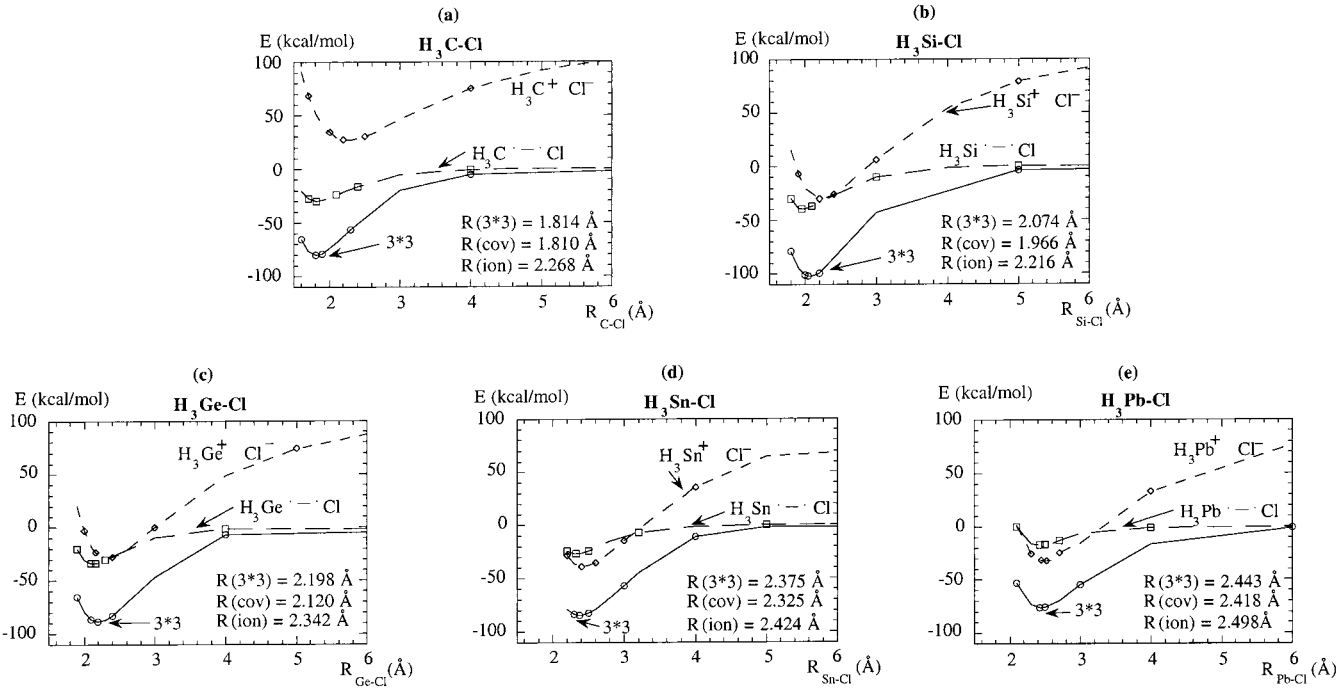

Figure 1. Computed VB energy curve along the M−Cl stretching coordinates for M = C → Pb in a−e, respectively. Shown are the SD-BOVB curves for the adiabatic 3 × 3 state along with the variationally optimized covalent and ionic curves for VB structures $\mathbf{1_d}$ and $\mathbf{2_d}$ (see Scheme 3). The well depth of the ionic curves relative to the asymptote (not shown) of the separated ions is 134.3, 164.1, 156.6, 160.1, and 149.0 kcal/mol for M = C, Si, Ge, Sn, and Pb, respectively.

Table 4. Weights and Coefficients for VB Structures **1** (Φ_{cov}), **2** ($\Phi_{ion}(M^+)$), and **3** ($\Phi_{ion}(M^-)$ of MH_3−Cl (M = C, Si, Ge, Sn, Pb)[a]

		weights			coefficients		
level	M	Φ_{cov}	$\Phi_{ion}(M^+)$	$\Phi_{ion}(M^-)$	Φ_{cov}	$\Phi_{ion}(M^+)$	$\Phi_{ion}(M^-)$
VBSCF	C	0.656	0.273	0.071	0.677	0.351	0.126
	Si	0.544	0.427	0.029	0.574	0.461	0.058
	Ge	0.558	0.408	0.034	0.593	0.465	0.057
	Sn	0.524	0.460	0.016	0.569	0.516	0.030
	Pb	0.515	0.471	0.014	0.592	0.536	0.027
L-BOVB	C	0.627	0.288	0.085	0.658	0.373	0.147
	Si	0.619	0.408	−0.027	0.681	0.438	−0.075
	Ge	0.581	0.397	0.022	0.602	0.459	0.070
	Sn	0.525	0.452	0.023	0.571	0.510	0.051
	Pb	0.513	0.465	0.022	0.568	0.533	0.052
SD-BOVB	C	0.656	0.269	0.075	0.704	0.397	0.133
	Si	0.619	0.384	−0.003	0.687	0.491	−0.081
	Ge	0.587	0.392	0.021	0.644	0.484	0.055
	Sn	0.539	0.448	0.013	0.607	0.534	0.042
	Pb	0.519	0.466	0.015	0.595	0.557	0.044

[a] All calculations refer to BSI.

always, D_{VBS} is identical with the variational covalent bond energies (D_{cov}) due to the spin-pairing of the two electrons.[4] It is seen that the covalent bond energies change in tune with the total bond energy, with a maximum for Si−Cl and a minimum for Pb−Cl or C−Cl. The same trend is observed in the D_{VBS} terms, as well as in the charge-shift resonance energies.

Even though generally the resonance energy increases as the VB level improves from VBSCF toward SD-BOVB, the percentage of the total bond energy contributed by RE_{cs} is virtually independent of the VB level. Moreover, the resonance energy is large and dominates the bond energy, being ∼65% of the total bond energy for all elements. The same picture is obtained by a direct VB-CI of the variationally optimized VB structures. In fact, in the 3 × 3 adiabatic state, the resonance energy is the sole major bonding event, giving virtually >90% of the total bond energy. As such, *the M−Cl bonds are neither covalent nor ionic but bonded by charge-shift resonance*.[5a−c]

Further support for this picture comes from the weights of the VB structures in Table 4, which we recall shows that starting with Si onward, the ionic weight is ∼40%, while for C the weight is significantly smaller. Further, the weights of the ionic structure do not seem to follow the trend exhibited by the covalent bond energies, by the charge-shift resonance energy, nor by the total bond energy. Importantly, the major covalent character of the C−Cl bond deduced from the structural weights conceals the fact that a major portion of the bonding is due to the charge-shift resonance, while Si−Cl with the highest charge-shift resonance energy does not possess the highest ionicity in the series. Indeed, as stated above, the bonds are neither covalent nor ionic; they are charge-shift bonds.

2 × 2 Covalent−Ionic Mixing: An Effective Model for Charge-Shift Bonding. To define the minimal effective model which still reproduces the trends in the total bond energies, we calculated bond energies using only the covalent structure $\mathbf{1}/\mathbf{1_d}$ and the lowest ionic structure $\mathbf{2}/\mathbf{2_d}$, hence $D_{2\times2}$. Table 6 compares $D_{2\times2}$ values with the total bond energy, $D_{3\times3}$, obtained with all three VB structures. It is seen that with SD-BOVB, as opposed to L-BOVB, the 2 × 2 model reproduces the trends and the orders of magnitude in the total bond energy. It follows therefore that a simple covalent−ionic mixing model of two configurations, with π-back-bonding, is required to account for the trends in total bond energy. A detailed analysis of the π-back-bonding effect in the two configurations shows that the effect is indeed maximal in SiH_3Cl. Thus, the ionic structure, $\mathbf{2_d}$, $\Phi_{ion}(M^+)$, exhibits a significant back-bonding effect which is largest for M = Si (10.8, 22.2, 19.4, 17.4, and 13.7 kcal/mol, respectively), and much the same is observed for covalent structure $\mathbf{1_d}$ (7.3, 14.9, 10.3, 7.0, and 4.7 kcal/mol, respectively), albeit to a smaller extent. The final π-bonding which is roughly an average of the contributions from the ionic and the covalent structures establishes the excess strength of the Si−Cl bond relative to its heavier analogues. Finally, testing for the relative contributions of the covalent bonding and charge-shift resonance

Table 5. Covalent Bond Energies, the Lowest Optimized VB Structure Bond Energies (D_{VBS}), and Charge-Shift Resonance Energies (RE_{cs})[a] of MH_3-Cl (M = C, Si, Ge, Sn, Pb) at Various Levels (kcal/mol)

	C		Si		Ge		Sn			Pb		
level	D_{VBS} (=D_{cov})	RE_{cs}	D_{VBS} (=D_{cov})	RE_{cs}	D_{VBS} (=D_{cov})	RE_{cs}	D_{cov}	D_{VBS}	RE_{cs}	D_{cov}	D_{VBS}	RE_{cs}
SD-BOVB	29.7	50.5	39.9	62.2	33.9	54.7	26.6	38.6	58.0	17.4	32.2	58.9
L-BOVB	23.8	46.0	27.6	58.4	25.2	51.2	20.1	20.1	54.2	13.0	15.5	54.5
VBSCF	23.8	37.7	27.6	52.1	25.2	46.7	20.1	20.1	49.7	13.0	15.5	50.0

[a] Calculated as the difference between the adiabatic and the optimized lowest VB structure curves at equilibrium distance. Using BSI.

Table 6. Bonding Energies (kcal/mol) with and without the Inverse Ionic Structure **3** ($\Phi_{ion}(M^-)$)

	L-BOVB			SD-BOVB		
	$D_{2\times2}$[a]	$D_{3\times3}$[b]	β_3[c]	$D_{2\times2}$[a]	$D_{3\times3}$[b]	β_3[c]
H_3C-Cl	60.2	69.4	−61.9	72.3	80.2	−58.5
H_3Si-Cl	75.8	83.4	101.4	92.9	101.2	101.7
H_3Ge-Cl	73.7	76.4	−38.4	86.2	88.6	−43.0
H_3Sn-Cl	72.8	74.2	−26.9	83.2	84.6	−32.8
H_3Pb-Cl	66.3	67.5	−24.1	75.0	76.3	−27.8

[a] The bonding energy due to the covalent structure **1** and the lowest ionic structure **2** ($\Phi_{ion}(M^+)$). [b] The bonding energy due to all three VB structures **1**, **2,** and **3**. [c] The reduced resonance integral between the 2 × 2 state and the inverse ionic structure **3** defined in eq 5 in the text.

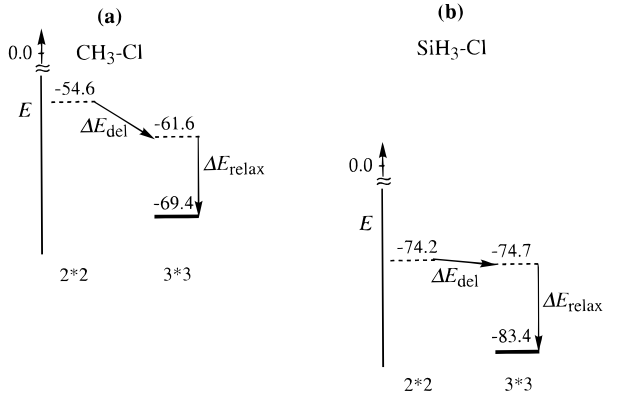

Figure 2. Effect of mixing of the inverse ionic structure, **3**, for CH_3-Cl (a) and SiH_3-Cl (b). The energies (kcal/mol) are relative to the separated radical fragments. In each case we show the 2 × 2 state due to the mixing of the two main structures (**1** and **2**) as well as the full 3 × 3 state. The ΔE_{del} shows the effect of mixing of **3** when the inactive lone pairs and M−H bonds are kept frozen in their forms in the 2 × 2 state. The ΔE_{relax} shows the effect of allowing the inactive electron pairs to relax and adapt themselves to the 3 × 3 mixing.

energy in a given bond confirms that, at the minimal effective 2 × 2 model too, the charge-shift resonance energy is the single most important contribution to the bond energy. *It follows, therefore, that charge-shift bonding is set by the two major VB structures which describe the bond.*

Let us turn now to elucidate the precise role of the third structure, $\Phi_{ion}(M^-)$, **3**/**3**$_d$, with the inverse ionicity. First, it is apparent from Table 6 that the bonds Ge−Cl, Sn−Cl, and Pb−Cl give a 2 × 2 bond energy which is essentially the same as the 3 × 3 value. Thus, these bonds are truly two-configuration bonds dominated by charge-shift bonding. In contrast, the inverse ionic structure has a significant effect on the bond energies of C−Cl and Si−Cl. To understand the effect of this third structure, we note that the traditional bond energy improvement of the ionic structures is associated with the increase in the delocalization of the active electrons by mixing with the covalent structure. Whenever this happens, we expect that the mixing coefficient of the ionic structures will be positive. However, turning back to Table 4, it is apparent that the mixing coefficient of **3**/**3**$_d$ is positive for all M−Cl bonds, but negative for Si−Cl. To appreciate better this "counterintuitive" effect, we show in Table 6 the reduced resonance integral β_3, which is the effective matrix element responsible for the mixing[4,45] of structure **3** into the 2 × 2 state, given by eq 5. The corresponding mixing coefficient is given by eq 6.

$$\beta_3 = H_{2\times2,3} - E_{2\times2}S_{2\times2,3} \quad (5)$$

$$c_3 = \beta_3/[E_{2\times2} - E_3] \quad (6)$$

$H_{2\times2,3}$ and $S_{2\times2,3}$ are the resonance integral and the overlap between the 2 × 2 state and the inverse ionic VB structure, **3**, respectively. $E_{2\times2}$ is the energy of the 2 × 2 state, while E_3 is the energy of the inverse ionic VB structure, **3**. Since the energy gap term in eq 6 ($[E_{2\times2} - E_3]$) is negative, the sign of the mixing coefficient will depend on the sign of the reduced resonance integral β_3.

This integral, which characterizes the interaction between a covalent structure and an ionic structure, *is normally negative* according to qualitative VB theory,[4,45] where it is assumed that both structures have similar orbitals and differ only by the occupancy of their active orbitals—those involved in the bond. The positive β_3 obtained for Si−Cl is an indicator that at the BOVB level the VB structures probably have significantly different inactive orbitals (which is indeed the case), and that therefore the β_3 integral is not dominated by the effect associated with delocalization of the bond pair, but rather by terms which are concerned with the relaxation of the inactive electron pairs. In contrast, in C−Cl which possesses a negative β_3 value, the inverse ionic structure, $H_3C^-Cl^+$, appears to fill its traditional role of delocalizing the active orbitals of the C−Cl bond.

The VB method enables one to test the idea by mixing the third VB structure while freezing the inactive orbitals and thereby turning off the effect of their relaxation. Figure 2 shows with dashed lines these "frozen" 2 × 2 and 3 × 3 energies, along with the fully relaxed 3 × 3 energies in bold, for C−Cl (in (a)) and Si−Cl (in (b)), all being L-BOVB data. The contribution due to delocalization of the active electrons can be judged by comparing the dashed lines in each case, while the relaxation of the inactive electrons can be read by comparing the 3 × 3 energies in the dashed and bold lines. By inspecting the dashed lines, for the 2 × 2 and 3 × 3 situations, it is seen that when the inactive electron pairs are frozen, the inverse-ionic configuration improves C−Cl bonding significantly (by 7.2 kcal/mol) by delocalizing the active electrons, and has virtually no effect on the Si−Cl bond energy (only 0.5 kcal/mol). Comparing now the energy of the 3 × 3 state in dashed and bold lines shows that the relaxation of the inactive electrons plays a significant role for C−Cl, but for Si−Cl the entire effect on bonding is due to the relaxation of the inactive pairs. Thus, the third configuration mixing in Si−Cl brings a dynamic correlation effect which is expressed when the inactive electrons are allowed to relax and adapt themselves better to the VB mixing.[46]

(45) Shaik, S.; Hiberty, P. C. *Adv. Quantum Chem.* **1995**, *26*, 99.

Scheme 4

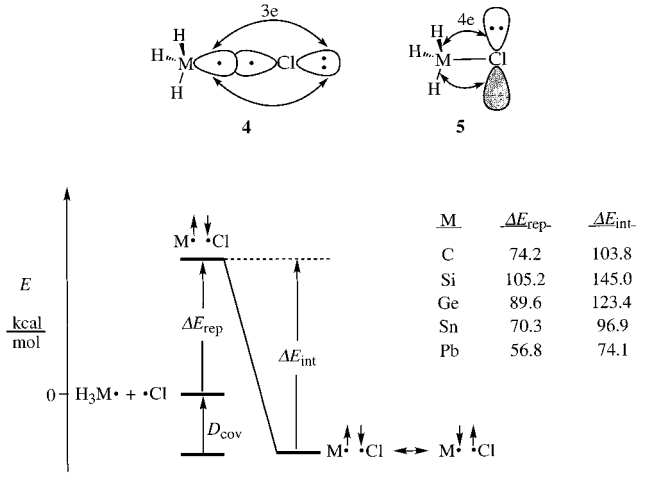

We may conclude therefore that the charge-shift bonding is an expression of primarily the mixing of the covalent, **1**/**1**$_{\mathbf{d}}$, and normal-ionic, **2**/**2**$_{\mathbf{d}}$, structures, especially for the bonds Si−Cl → Pb−Cl.

B. Factors of Charge-Shift Bonding: Energy and Structural Patterns of the Major VB Structures. Having established the charge shift in terms of two VB structures, we turn to comprehend their behavior and mixing patterns.

Bond Weakening in the Covalent Structure. The covalent bond energies, D_{cov}, collected in Table 5 behave in a nonmonotonic manner and seem curiously small, especially for C−Cl. This bond-weakening effect has been discussed by Sanderson[47] and has been shown by two of us[5a,b,48a] to originate in repulsion between the σ-lone pair and the bond pair as shown in **4** in Scheme 4, augmented by the repulsion between the π-lone pair and M−H orbitals in **5**. VB theory enables a direct assessment of the repulsive interactions[48a] by calculating the energy of one of the constituent spin determinants[4] such that the covalent interaction energy due to the spin exchange (**a** in Scheme 1) is turned off. The results are depicted in the lower part of Scheme 4, where the zero energy reference is the sum of the fragment energies at infinity. It is seen that the covalent bond energy is a balance between the interaction energy due to the spin exchange and a nonbonded repulsive energy (as depicted in **4** and **5**) that is particularly large. The net result is a severely weakened covalent M−Cl bond. To appreciate the significant bond-weakening effect due to the lone-pair/bond-pair repulsion in the H_3M−Cl molecules, the repulsive energy of H_3M−Cl in Scheme 4 can be compared with the much smaller value, ca. 56.5 kcal/mol, in H_3C−CH_3, which is devoid of lone pairs.[48b]

In summary, the covalent structure is weakened in all the bonds, so that significant bond energy can arise only if the ionic structure is low enough in energy or can mix strongly to provide the charge-shift bonding. Let us turn to consider the ionic structure.

Scheme 5

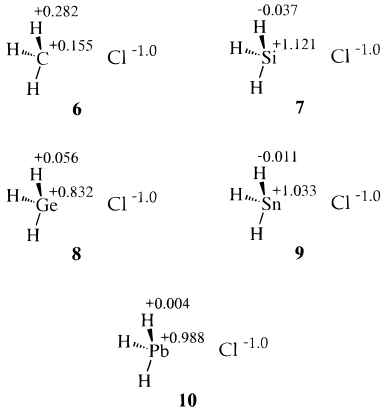

Stabilizing Factors of the Ionic Structure. As noted in the Results, the ionic curves in Figure 1 exhibit very deep wells, 134, 164, 157, 159, and 149 kcal/mol for CH_3Cl, SiH_3Cl, GeH_3Cl, SnH_3Cl, and PbH_3Cl, respectively. The same trend is obtained from point charge calculations of the electrostatic interactions within the ionic structures themselves. The fact that $SiH_3^+Cl^-$ exhibits the deepest well while $CH_3^+Cl^-$ the shallowest does not follow from any obvious intuitive property of the group IVB atoms, and requires elucidation.

Mulliken population analysis performed on the ionic structures and presented in **6**−**10** in Scheme 5 provides the root cause of the above behavior. The positive charge localization on the M center is the lowest on carbon and the highest on silicon, and this trend by itself is sufficient to account for the well depth of the ionic curves. Thus, $CH_3^+Cl^-$ (**6**) with the lowest charge on M has the shallowest well, while $SiH_3^+Cl^-$ (**6**) with the highest charge possesses the deepest well.

It is interesting to note that the positive charge localization on M exhibits a saw-tooth behavior; starting very low in $CH_3^+Cl^-$ (**6**), shooting up in $SiH_3^+Cl^-$ (**7**), decreasing again to an intermediate value in $GeH_3^+Cl^-$ (**8**), increasing again in $SnH_3^+Cl^-$ (**9**), and decreasing in $PbH_3^+Cl^-$ (**10**). The major effect on this trend is set by the electronegativity of the group IVB atoms relative to H. Thus, as we move down the IVB group elements, the valence orbitals increase in size and their energies go up, with a consequential decrease of electronegativity.[44] Two secondary effects,[9,29] overlayed on this major trend, are the transition metal contraction in Ge, and the lanthanide and relativistic contractions in Pb,[29] which decrease the size and energy of especially the ns valence orbitals, thereby creating a zigzag behavior of the electronegativity and hence of M's capability to sustain a positive charge in MH_3^+. Since we are considering the cations in their pyramidal geometry (pertaining to the ground-state structure), the MH_3^+ species are sp^n hybridized, and these secondary effects are accentuated due to the participation of the s orbital. Thus, the similar electronegativities of C and H lead to positive charge delocalization. As we move on to Si, a sharp drop in silicon's electronegativity results in a sharp increase of the positive charge on Si. Continuing to Ge, the effect of transition metal contraction makes Ge more electronegative than Si, and lowers the charge localization on Ge. Descending further to Sn, the electronegativity decreases again and the charge localization on Sn accordingly increases again. Finally, moving on to Pb, the lanthanide and relativistic contractions raise the electronegativity and the charge localization on Pb decreases again.

(46) Strictly speaking, if the inactive orbitals of the various BOVB configurations are more different from what would be required by the mere breathing orbital effect that just adapts the shape of the orbitals to the charge fluctuation, part of the energy stabilization contributed by the mixing of the inverse ionic structure, *but not all of it*, could well be a bias due to correlation of the inactive pairs in the molecule but not in the fragments. It is not possible to quantify the precise magnitude of the bias, and in any event, it is clear that in the present situation it cannot be large.

(47) Sanderson, R. T. *Polar Covalence*; Academic Press: New York, 1983.

(48) (a) Lauvergnat, D.; Hiberty, P. C. *J. Mol. Struct (THEOCHEM)* **1995**, *338*, 283. (b) Shurki, A. Unpublished BOVB calculations using basis set BSI. Note that in ref 48a the repulsion energy (e.g., 17 kcal/mol for CH_3CH_3) is calculated relative to a reference where the orbitals of the fragments are frozen as those possessed in the covalent structure. In the present work the orbitals of the fragments are the relaxed SCF orbitals, and as such our ΔE_{rep} term contains the orbital relaxation effect of the fragments.

Scheme 6

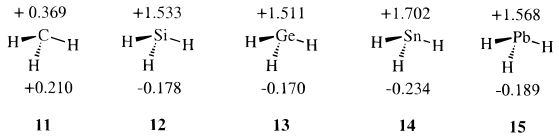

Table 7. Covalent and Ionic Radii of H_3M Fragments (M = C, Si, Ge, Sn, Pb)

level	M = C	M = Si	M = Ge	M = Sn	M = Pb
		Covalent Radii ($H_3M^{\bullet}$)[a]			
BSI[b]	0.82	0.98	1.13	1.33	1.43
BSII[c]	0.84	0.99	1.14	1.34	
Pauling[d]	0.77	1.17	1.22	1.40	
		Ionic Radii (H_3M^+)[a]			
BSI[b]	0.46	0.41	0.53	0.61	0.69
BSII[c]	0.67	0.31	0.70	0.78	
Pauling[d]	0.29	0.65	0.76	0.96	

[a] r_{Cl} = 0.99 Å; r_{Cl^-} = 1.81 Å taken from pages 224, and 514, respectively in ref 2. [b] Calculated at the SD-BOVB level. [c] Calculated at the D-BOVB level. [d] Reference 2.

The same trends are obtained from an NBO analysis of the free MH_3^+ cations, shown in Scheme 6. Much like the data in Scheme 5, the NBO analysis predicts equal distribution of the positive charge between the C and the hydrogens, while for the rest of the elements (Si, Ge, Sn, Pb), it predicts all the positive charge to be virtually on the M atom. Furthermore, much like in Scheme 5, here too the M charge exhibits a saw-tooth pattern.

Hand in hand with the charge localization on M, which occurs from Si onward, the doubly occupied inactive orbitals of MH_3^+ will tend to be localized more toward the H, and will therefore minimize the closed-shell repulsion with the Cl^- anion. Thus, the charge localization trends and the accompanying weakening of closed shell repulsion in the $MH_3^+Cl^-$ structure account for the trends in the depth of the corresponding ionic curves in Figure 1.

Another expression of the positive charge localization on the MH_3^+ cations is manifested in their effective size for their close-contact interaction with Cl^-. This effect can be ascertained by comparing the location of the minima for the ionic and covalent curves in Figure 1 and Table 1. It is seen that, for C−Cl, the ionic minimum is longer than the covalent minimum by ∼0.46 Å, whereas for the rest of the M−Cl bonds, the two curve minima are much closer (0.25, 0.22, 0.10, and 0.08 Å, respectively). Moreover, the ionic minimum of the C−Cl is longer than the corresponding minimum of Si. To see more clearly the reason for the different behavior of the ionic curves, we turn to quantify the effective radii of the radicals ($MH_3^{\bullet}$) and the cations (MH_3^+). The VB method enables one to do so by assuming that the minimum of the covalent curve is expressed as a sum of the covalent radii, while the minimum of the ionic curve corresponds to the sum of the ionic radii (the radii of $Cl^{\bullet}$ and Cl^- taken as the known quantities[2]).

These data are collected in Table 7 for both BSI and BSII basis sets[35,49] alongside the corresponding Pauling values. It is seen that the covalent radii calculated at the two different basis sets are almost identical, both showing the same trend as expected with Pauling's values, that the covalent radii increase as M becomes heavier. In contrast, the calculated ionic radii deviate from the trend predicted by Pauling's values and exhibit a completely different picture. The ionic radii calculated using BSI are shown to be in most cases smaller than those calculated using BSII except for the SiH_3^+ radii, which are predicted to be especially small according to BSII calculations. Despite the different numerical results, the two basis sets exhibit the same trend; namely, the ionic radius of SiH_3^+ is the smallest, while those of CH_3^+, GeH_3^+, SnH_3^+, and PbH_3^+ are either similar or increase monotonically and slowly from the lightest to the heaviest. These results, surprising as they may be, appear to be in good agreement with the charge analysis in the ionic structure in Schemes 5 and 6. Thus, a large positive charge on M will shrink the MH_3^+ ion relative to the corresponding $MH_3^{\bullet}$ radical and will create a smaller effective size along the missing coordination site of MH_3^+. The weakest shrinkage effect occurs for CH_3^+ due to the delocalized charge. SiH_3^+ with the largest Si-localized positive charge undergoes the highest percentage of shrinkage and becomes the smallest cation. The other cations with somewhat smaller localized charges on M undergo smaller percentages of shrinkage, and since the corresponding radicals are to begin with large, the size shrinkage leaves these cations larger than or of the same size as CH_3^+.

(49) The BSI results are given at the SD-BOVB level whereas the BSII results refer to the D-BOVB level; however, preliminary examination showed that the split does not effect the shape of the curves (i.e., the minimum of the curves does not change due to splitting).

Table 8. Bond Energies (kcal/mol) Obtained by Mixing of $\mathbf{1_d}$, Φ_{cov} with $\mathbf{2_d}$, $\Phi_{ion}(M^+)$ at the SD-BOVB Level[a]

		variationally optimized Φ_{cov} and $\Phi_{ion}(M^+)$			adiabatic 2 × 2 mixing		
entry	M	D_{cov}	*RE*	$D_{2\times2}$	D_{cov}	*RE*	$D_{2\times2}$
1	C	29.6	26.4	56.0	2.6	69.7	72.3
2	Si	39.6	40.7	80.4	−9.1	102.0	92.9
3	Ge	33.0	40.9	73.9	8.6	77.6	86.2
4	Sn	26.2	47.2	73.4	4.4	78.8	83.2
5	Pb	17.3	48.9	66.2	−0.1	75.5	75.4

[a] All calculations are performed at the *R*(M−Cl) obtained at the 3 × 3 adiabatic level.

The foregoing trends show that the covalent bond weakening and the deep and tight ionic structures act cooperatively to create large charge-shift resonance energies. The effect is weakest for C, larger for all the heavier elements, and maximum for Si. Thus, the small size of the SiH_3^+ ion creates an ionic curve, $SiH_3^+Cl^-$, with a very tight minimum which approaches the covalent minimum, hence minimizing the configuration energy gap, maximizing the configuration mixing matrix element, and optimizing thereby the charge-shift resonance energy. This picture reinforces the status of Φ_{cov} and $\Phi_{ion}(M^+)$ as the essential constituents of charge-shift bonding.

As a final means of assessing the special status of the charge-shift bonding, we collected in Table 8 bond energies at the 2 × 2 D-BOVB level, under two different orbital optimization conditions. The left part of the table presents data for a situation where the two variationally optimized VB forms mix, as such, to generate the 2 × 2 bond state. In the right-hand part of the table, we show the 2 × 2 energetics when the two VB structures are allowed to adapt themselves to the VB mixing. It is seen clearly that, upon adaptation to the VB mixing, the covalent bonding has diminished significantly and become even negative for Si−Cl. A similar fate is met by the ionic structure, which rises in energy in the adiabatic 2 × 2 calculations. We were further able to ascertain that the *energy rise of the ionic structure is not due to a change in the electrostatic interactions, but due to orbital distortion*. The orbital distortion is expressed by an almost 2-fold reduction of the overlap between the covalent and ionic forms. Thus, in the adiabatic 2 × 2 mixing the two VB structures rise in energy due to orbital distortions, and nevertheless, the total bond energies increase significantly. This is seen to be the result of an overwhelming increase in the charge-shift resonance energy. It follows, therefore, that *the individual VB*

structures sacrifice their lowest possible energies in favor of intensifying the charge-shift resonance energy, and acquiring thereby an improved bond energy. Thus, as we already noted, the target bonds of this study are neither covalent nor ionic, but rather an oscillating mixture of the two forms which we proposed to call charge-shift bonding. This definition certainly fits perfectly all the bonds from Si−Cl downward to Pb−Cl, while less so for the C−Cl bond, which appears to be a borderline case between the traditional polar covalent bond and the charge-shift bond.

C. Manifestations of Charge-Shift Bonding. Ionic Chemistry. As noted in the Introduction, the solid-phase ionic chemistry of Si and other heavy elements in group VIB is rare,[14,18−21] in contrast to the well-established ionic chemistry of C.[13,15] In a recent study of CH_3Cl and SiH_3Cl, it has been suggested[5c] that part of this behavior originates in the charge localization of the two cations. Thus, in a CR_3^+ cation the positive charge is well delocalized, and therefore the cation is sensed by the negative counterion as a large object with roughly uniform charge distribution. This property will favor the formation of ionic crystals $CR_3^+X^-$, where electrostatic energy is maximized by surrounding each ion by a few close neigboring counterions which maintain multidirectional electrostatic stabilization.

In contrast, the SiR_3^+ cation has a large positive charge on the Si and negative charge on the R groups (Scheme 5). Thus, the SiR_3^+ cation looks like a doughnut which possesses a positively charged hole in the center surrounded by a rim of negative charge. This means that SiR_3^+ cations will possess a small effective size along the missing coordination site and a large size otherwise. In a putative ionic solid which is characterized by periodic multidirectional electrostatic interactions (Madelung energy), a doughnut-like cation with a negative rim will not enjoy this Madelung energy. Instead, the small effective size of SiR_3^+ will create *structural directionality* by permitting a close approach of the counterion X^-, with concomitantly strong and unidirectional electrostatic interaction. As a consequence, the ionic curve will approach the covalent curve, a situation which results in a significant charge-shift resonance bonding energy. In such a 1:1 species, even though the charge distribution in the Si−X bond may still appear ionic, this ionicity will remain virtual. Thus, SiR_3−X prefers to form discrete molecular structures, each of which is stabilized by charge-shift resonance rather than a periodic ionic solid which enjoys multidirectional electrostatic stabilization. A similar situation will be exhibited by SnR_3^+ cations,[22] and somewhat less so by GeR_3^+ and PbR_3^+ cations,[50] due to the effects[29] of transition metal contraction and the relativistic contraction. Even though the situation is more complex in the solution phase, still similar effects can be the root cause of the fleeting existence of solvated MR_3^+ (M = Si, Sn) cations.[17,22] Thus, we propose that due to charge-shift bonding these cations, e.g., *SiR_3^+, will prefer to form in solution discrete structures, in which electron-rich ligands (e.g., solvent molecules) approach the cation along the missing coordination site and form, e.g., trigonal bipyramidal structures.* Similar views, based on different considerations, have been expressed by the main research groups in the area.[14,18−21]

Of course, one might devise SiL_3^+ cations where the charge is delocalized (e.g., L = SiR_3, SnR_3, PbR_3, GeR_3). In such cations *the effective size of the Si cation will increase*, but the rim of negative charge will still surround the cationic centers. Consequently, one may predict that bonds such as $Si(SiR'_3)_3$−Cl or $Si(SnR'_3)_3$−Cl will become considerably weaker due to diminished charge-shift resonance energy. However, the negative rim may still impair the formation of ionic crystals, or solvated SiL_3^+ cations. Recent advances have shown in the meantime how to generate such ions by steric protection of the Si center.[21] It remains a challenge to design such ions without the steric protection. To do so, it is essential to devise a charge-delocalized SiR_3^+ cation *without a rim of negative charge*. On the basis of the charge distribution patterns in Scheme 5, the best chances to avoid the negative rim is to use cations such as $Si(GeR'_3)^+$.

Scheme 7

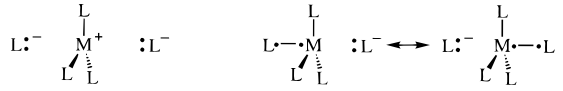

16 **17**

Hypercoordination Chemistry. The ubiquity of hypercoordination compounds ML_n ($n > 4$), especially for M = Si and Sn,[26] is associated with charge-shift bonding. In a recent study, Reed and Schleyer[27] have shown that the central atom in the hypercoordinated compound carries a high positive charge. While this is certainly a major aspect, we recall that hypercoordinated compounds are not really ionic and hypercoordination is in essence a resonating mixture of an ionic form and a covalent form, stabilized by a large charge-shift resonance interaction.[5e,45,51,52]

Consider for example these VB structures, shown in Scheme 7, for an ML_5^- pentacoordination. The pentacoordinated ionic structure, depicted in **16**, is strongly stabilized for M = Si, and M = Sn due to the intensified electrostatic interaction contributed by (i) the small effective size of the ML_3^+ cation which enables a close approach of the L^- anion along the vacant axis, (ii) the charge concentration on M, and (iii) the aggregated electrostatic interactions due to the presence of the two counteranions. The complementary effect is the resonance energy due to mixing with the covalent structure **17**. This large resonance energy carries over from the normal-valent molecule, and serves to generate a charge-shift-bonded hypercoordinated species. This effect will be strongest for Si and Sn, somewhat less so in Ge and Pb due to the $3d^{10}$ and relativistic contraction effects discussed above for the latter elements, and weakest for C. A well-established trend is known from the S_N2 chemistry of Si vs C,[10a,45,52] where Si forms stable pentacoordinated intermediates as opposed to C, which forms only unstable transition states. Not much is known about the S_N2 process of the other elements, and this may be worthy of future pursuit.

Conclusions

Charge-shift bonding is not associated with either the covalency or ionicity of a given bond, *but derives, primarily if not only, from the fluctuation of charge inherent in the resonance between the two bonding forms* (**a** and **b** in Scheme 1).[7] The VB computations of the M−Cl bond (M = C, Si, Ge, Sn, Pb) demonstrate that all the bonds from Si−Cl downward are strictly charge-shift bound, while C−Cl seems to be a borderline situation between a traditional covalent-polar bond and a charge-shift bond.

(50) Frenking, G.; Fau, S.; Marchand, C. M.; Grützmacher, H. *J. Am. Chem. Soc.* **1997**, *119*, 6648.

(51) Epiotis, N. D. Unified Valence Bond Theory of Electronic Structure. Applications. *Lect. Notes Chem.* **1983**, *34*, 265−285.

(52) **.** Shaik, S. In *Encyclopedia of Computational Chemistry;* Schleyer, P. v. R., Allinger, N. L., Clark, T., Gasteiger, J., Kollman, P. A., Schaefer, H. F., III, Eds.; John Wiley: Chichester, U.K., 1998; Vol. 5, pp 3143−3156.

The charge-shift character of the above bonds is shown to originate in two factors. The first is the weakening of the covalent bonding, $H_3M^{\bullet} - {}^{\bullet}Cl$ (**1**), due to repulsion of the bonding electrons with the lone pair on Cl and the nonbonded repulsion of the inactive electron pairs.[5,47,48] This covalent bond weakening means that any strong bonding will have to arise from the resonance between the covalent and ionic, $H_3M^+:Cl^-$ (**2**), forms. Here enters the second factor, expressed mainly through the ionic structure $H_3M^+:Cl^-$ (**2**), where the smaller M electronegativity relative to H imposes positive charge localization on the M center, and thereby induces enhanced electrostatic stabilization of the ionic structure. The two factors minimize the energy gap between the VB structures, increase their reduced matrix element, and maximize their interaction resonance energy, thereby creating bonds which are sustained mainly by the charge-shift resonance.

The positive charge localization in MH_3^+ appears to be a key factor leading to charge-shift bonds with strong bonding energy. The charge localization property exhibits a saw-tooth behavior, starting small for M = C, rising to a maximum for M = Si, and then alternating down and up from M = Ge toward M = Pb. It is shown that the pattern is associated with the transition metal contraction due to imperfect screening of the $3d^{10}$ shell in Ge, and the lanthanide and relativistic contractions[29] in Pb. These two effects cause a zigzag variation in the electronegativity of M, which is expressed through the charge localization pattern in the MH_3^+ cations. The cation with the highest charge localization is SiH_3^+, which leads to the strongest Si−Cl bond, while the cation with the highest charge delocalization is CH_3^+, which is associated with the weakest or second weakest bond. A consequence of the charge localization is the finding that SiH_3^+ possesses the smallest ionic radius.

Charge-shift bonding is manifested in (a) rare ionic chemistry and free R_3M^+ cations for M = Si → Pb and (b) the tendency of Si and Sn (and less so of Ge and Pb) to form hypercoordination.

An alternative approach to the VB analysis present here is the method developed by Bickelhaupt et al.[12b,58] The method uses a density functional component analysis which resembles a Morokuma[59] analysis performed on a density made from Kohn−Sham orbitals. The analysis of Bickelhaupt et al.[12b] shows that the bond energy is a balance of a steric repulsion (Pauli repulsion) term and an orbital interaction term. The steric term may be associated with the VB derived bond-weakening effect in Scheme 4. Similarly, the orbital interaction term can be equated with the sum of covalent and charge-shift bonding contributions in the VB approach. Indeed the numerical quantities which emerge from the two approaches exhibit similar trends. While equivalence of the two approaches can be established, the present VB analysis projects with better lucidity the dominant role of charge-shift bonding in these bonds.

Charge-shift bonding appears in homonuclear as well as heteronuclear bonds, and hence is a complementary paradigm to the covalent and ionic ones already entrenched in chemical epistemology. Its appearance in a variety of molecules, e.g., X−F (X = F, H, CH_3, SiH_3),[5a,b] HO−OH,[5b] CH_3−OH,[6] H_2N−NH_2,[5b] and CH_3−NH_2,[6] in ion−molecule bonds as in the CH_3−NH_3^+ species,[5d] in hypercoordinated species and transition structures, e.g., $(FHF)^-$,[5e] $(FCH_3F)^-$, and $(FSiH_3F)^-$,[5b,45,52] as well as in the present series of molecules, shows that this type of bonding is not restricted to a small set of molecules. Furthermore, the root causes for the formation of charge-shift bonding (repulsion of bonds by lone pairs, nonbonded repulsions and compact bond orbitals[5b]), which are so common, suggest that it might prove to be a ubiquitous bonding flavor in chemistry. We are looking forward to recognizing additional manifestations of this bonding mechanism in structure and reactivity.

Appendix. Practical Procedures in BOVB Calculations

L-BOVB. At this level, the orbitals of each fragments are kept fully localized either on Cl or on MH_3. Except for the core orbitals that can optionally be specified as common to all VB structures in all-electron basis sets, all other orbitals of the VB structures **1, 2**, and **3** are specified as independent orbitals in the wave functions. To start the calculations with convenient guess orbitals, one may take the orbitals of the isolated $MH_3^{\bullet}$ and $Cl^{\bullet}$ fragments for the covalent structure, and the corresponding anions or cations for the ionic structures. Letting then the various orbitals and coefficients of the VB structures optimize simultaneously to minimize the energy of the 3 × 3 ground state leads to the L-BOVB wave function.

SL-BOVB. At this level the doubly occupied active orbital of each ionic structure is split into two singly occupied orbitals of different sizes and shapes (see drawings below). Therefore,

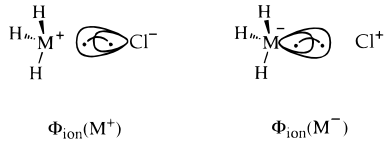

this level requires reoptimization of the active orbitals. Since some of the inactive orbitals (e.g., the σ-lone pair on Cl) possess the same symmetry as the active orbitals, it is necessary to ascertain that the split orbitals remain the active ones and do not switch in the process of optimization to, e.g., some lone pair of the inactive set. This is achieved by first localizing the active and inactive orbitals, arising from the L-BOVB calculation, using the Boys localization procedure (note that this procedure requires preliminary orthogonalization of the orbitals within each fragment). Then, the active doubly occupied orbital is identified as the hybrid pointing in the bond direction, and there remains to split this active orbital and optimize the resulting orbital pair. At the same time the inactive orbitals are kept frozen, to prevent any switching between active and inactive sets.

The corresponding SL-BOVB wave function is still made of three VB structures, but each ionic structure involves now two determinants which account for the singlet pairing of the electron pair in the split orbital (see the drawing). While the direct optimization of this wave function is possible, experience has shown us that it is not easy to find guess orbitals for ionic

(53) (a) For H_3C−Cl see: *J. Phys. Chem. Ref. Data* **1974**, *3*, 392. (b) For H_3Si−Cl see: *J. Phys. Chem. Ref. Data* **1982**, *11*, 745. (c) For H_3Ge−Cl see: Cradock, S.; McKean, D. C.; MacKIenzie, M. W. *J. Mol. Struct.* **1981**, *74*, 265. (d) For H_3Sn−Cl see: Bürger, H.; Betzel, M.; Schulz, P. *J. Mol. Spectrosc.* **1987**, *121*, 218.

(54) (a) Curtiss, L. A.; Raghavachari, K.; Trucks, G. W.; Pople, J. A. *J. Chem. Phys.* **1991**, *94*, 7221. (b) Pople, J. A.; Head-Gordon, M.; Fox, D. J.; Raghavachari, K.; Curtiss, L. A. *J. Chem. Phys.* **1989**, *90*, 5622.

(55) Lias, S. G.; Bartmess, J. E.; Liebman, J. F.; Holmes, J. L.; Levin, R. D.; Mallard, W. G. *J. Phys. Chem. Ref. Data* **1988**, *17*, Suppl. No. 1.

(56) Walsh, R. *Acc. Chem. Res.* **1981**, *14*, 246.

(57) Jackson, R. A. Special Publication No. 24, The Chemical Society, 1970, p 295. Taken from *Free Radicals*; Kochi, J. K., Ed.; Wiley and Sons: New York, Vol. 2, Chapter 25, p 743. Assuming that the influence of the R group which is attached to the M central atom on the strength of the M−Cl bond will be small and similar for all, one can see the same trend predicted by the calculations.

(58) Bickelhaupt, F. M.; Nibbering, N. M. M.; van Wezenbeeck, E. M.; Baerends, E. J. *J. Phys. Chem.* **1992**, *96*, 4864.

(59) Kitaura, K.; Morokuma, K. *Int. J. Quantum Chem.* **1976**, *10*, 325.

structures with split orbitals. It is much easier to proceed in an indirect way, using the fact that a single ionic structure with split active orbitals is equivalent to a combination of two ionic structures of closed-shell forms, which differ by the shape of their doubly occupied active orbital: one being nodeless, the other having a node. The practical procedure is thus as follows: (a) Each ionic structure is doubled, and a node is artificially created in the active orbital of one of them, to create an ad-hoc guess orbital. Then the orbitals and coefficients of the resulting five-structure VB wave function are optimized, with excellent convergence in general. (b) Upon convergence, each two-configuration ionic VB structure is converted to a single VB structure displaying a split active orbital as illustrated above. This transformation is exactly equivalent to the transformation of σ_g and σ_u natural orbitals to a (χ_l, χ_r) GVB pair in a GVB calculation. Note that the transformation of the five-structure wave function to the final three-structure one is not necessary if one is only interested in the energy, which is exactly the same within both representations.

SD-BOVB. The inactive orbitals are now allowed to delocalize over the whole molecule, while the active orbitals remain localized on their respective fragment. Much as in the case of orbital splitting, in the delocalization procedure too, it is important to avoid switching or mixing between the active and inactive orbital sets. Thus, the delocalization is performed by reoptimizing only the inactive orbitals, while the active orbitals are kept frozen and localized in their L-BOVB or SL-BOVB forms.

Acknowledgment. We are grateful to J. H. van Lenthe and C. P. Byrman for making TURTLE available, to D. Lauvergnat for assistance in applying the BOVB method, and to M. Dolg for advice on aspects concerning the ECP in ref 35b. The research at the Hebrew University is supported by the ISF established by the Israeli Academy of Sciences and Humanities.

JA982218F